IL NUOVO CIMENTO **44 C** (2021) 179
DOI 10.1393/ncc/i2021-21179-1

COLLOQUIA: La Thuile 2021

Neutrino quantum decoherence at reactor experiments

C. A. TERNES(*)

Istituto Nazionale di Fisica Nucleare (INFN), Sezione di Torino
Via P. Giuria 1, I-10125 Torino, Italy

received 16 September 2021

Summary. — Using most recent data from reactor experiments we derive the presently best bound on the neutrino wave-packet width and show the robustness of the measurement of the standard oscillation parameters. We also discuss how much JUNO can improve this bound.

1. – Introduction

The topic of this talk is the in-flight loss of coherence of neutrinos. Neutrino mixing arises as a consequence of the non-diagonality of charged-current weak interactions for both charged leptons and neutrinos. Neutrino flavor eigenstates are produced in charged current interactions and can be written as coherent quantum superpositions of the mass eigenstates, $\nu_\alpha = \sum_i U_{\alpha i}\nu_i$. Since neutrinos have different masses, the wave-packets associated to each of the mass eigenstates may propagate with different velocities. After some time the wave-packets would not overlap anymore and oscillations are suppressed. The talk is based on refs. [1] and [2].

2. – Neutrino oscillations with decoherence

Reactor antineutrino experiments measure the disappearance of $\overline{\nu}_e$. The survival probability, including decoherence effects, is simply [3, 4]

$$P^{\rm dec}(\overline{\nu}_e \to \overline{\nu}_e) = \sum_{j,k} |U_{ej}|^2 |U_{ek}|^2 \, \exp[-i\Delta_{jk} - \xi_{jk}] \,, \tag{1}$$

(*) E-mail: ternes@to.infn.it

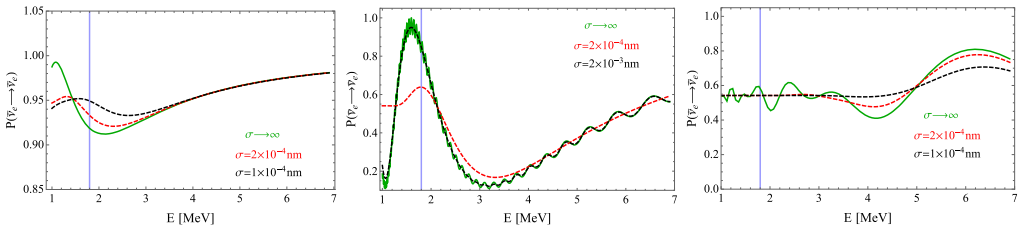

Fig. 1. – The $\overline{\nu}_e$-survival probability without decoherence effects (green) and for several finite values of the wave-packet width (black and red). Standard oscillation parameters are set to their best fit value, taken from ref. [7]. The left panel corresponds to a baseline of 1 km, relevant for Daya Bay and RENO, the central panel depicts the probability for JUNO for $L = 52.5$ km and the right panel for the characteristic baseline for KamLAND (which is an average over several baselines).

where

$$\Delta_{jk} \equiv 2\pi \frac{L}{L^{\rm osc}_{jk}} \equiv \frac{\Delta m^2_{jk} L}{2E}\,, \tag{2}$$

with $\Delta m^2_{jk} = m^2_j - m^2_k$ is the standard oscillation phase. The second term, $\xi_{jk}(L,E) = \xi_{kj}(L,E)$, quantifies the loss of coherence as a function of the neutrino energy E and the baseline L. It is given by

$$\xi_{jk}(L,E) = \left(\frac{L}{L^{\rm coh}_{jk}}\right)^2, \tag{3}$$

with the coherence lengths [4-6]

$$L^{\rm coh}_{jk} = \frac{4\sqrt{2}E^2}{|\Delta m^2_{jk}|}\sigma\,. \tag{4}$$

Here, σ is the width of the neutrino wave-packet. The survival probability for different baselines and different values of σ is shown in fig. 1. The left panel corresponds to a baseline of $L = 1$ km, while the central panel is obtained for $L = 52.5$ km. These are the relevant baselines for the short baseline experiments RENO and Daya Bay and the future medium baseline experiment JUNO, respectively. As can be seen from the plots the inclusion of finite decoherence effects results in a suppression of the oscillation amplitudes and also in a shift of the position of the oscillation minima. In the panel corresponding to JUNO we see that the fast oscillations (the oscillations due to the atmospheric mass splitting) are washed out first. The right panel corresponds to an effective (averaged) oscillation probability as observed in KamLAND. KamLAND measured the flux from several reactors at baselines ranging from $\mathcal{O}(100$ km)–$\mathcal{O}(1000$ km). Due to the long baselines, matter effects have to be included in the calculation of the survival probability. These matter effects do not affect the decoherence parameter [4]. However, the standard oscillation parameters have to be replaced by their matter counterparts. We use the parameterization discussed in ref. [8], which has been shown to be among the most precise and most efficient ones [9].

3. – Results from current experiments

We analyzed data from several reactor experiments. We include the most recent data sets from Daya Bay [10] and RENO [11]. Regarding KamLAND we use data publicly available in ref. [12], which correspond to the analysis of ref. [13].

In our statistical analysis, we include systematic uncertainties related to the thermal power for each core and to the detection efficiencies, uncertainties on the fission fractions, a shape uncertainty for each energy bin in our analyses, and an uncertainty on the energy scale. We define the χ^2 function for RENO as

$$\chi^2_{\rm RENO}(\vec{p}) = \min_{\vec{\alpha}} \left\{ \sum_{i=1}^{N_{\rm RENO}} \left(\frac{R^{F/N}_{{\rm dat},i} - R^{F/N}_{{\rm exp},i}(\vec{p},\vec{\alpha})}{\sigma_i^{\rm RENO}} \right)^2 + \sum_k \left(\frac{\alpha_k - \mu_k}{\sigma_k} \right)^2 \right\} . \tag{5}$$

Here, $R_i^{F/N} = F_i/N_i$, where F_i and N_i are the event numbers in the ith energy bin at the far and near detector, respectively. $R_{{\rm dat},i}$ are the background-subtracted observed event ratios, while $R_{{\rm exp},i}(\vec{p},\vec{\alpha})$ are the expected event ratios for a given set of oscillation parameters $\vec{p}$. The uncertainty for each bin is given by $\sigma_i^{\rm RENO}$. The last term contains penalty factors for all of the systematic uncertainties α_k with expectation value μ_k and standard deviation σ_k. Finally the number of bins is given by $N_{\rm RENO}$. Similarly, we define

$$\chi^2_{\rm DB}(\vec{p}) = \min_{\vec{\alpha}} \left\{ \sum_{i=1}^{N_{\rm DB}} \left(\frac{R^{F/N_1}_{{\rm dat},i} - R^{F/N_1}_{{\rm exp},i}(\vec{p},\vec{\alpha})}{\sigma_i^{F/N_1}} \right)^2 + \sum_{i=1}^{N_{\rm DB}} \left(\frac{R^{N_2/N_1}_{{\rm dat},i} - R^{N_2/N_1}_{{\rm exp},i}(\vec{p},\vec{\alpha})}{\sigma_i^{N_2/N_1}} \right)^2 + \sum_k \left(\frac{\alpha_k - \mu_k}{\sigma_k} \right)^2 \right\} . \tag{6}$$

for Daya Bay, where we take the ratios of the experimental hall 3 (F) to experimental hall 1 (N_1) and between experimental halls 2 (N_2) and 1. Finally, we have

$$\chi^2_{\rm KL}(\vec{p}) = \min_{\vec{\alpha}} \left\{ \sum_{i=1}^{N_{\rm KL}} \left(\frac{N_{{\rm dat},i} - N_{{\rm exp},i}(\vec{p},\vec{\alpha})}{\sigma_i^{\rm KL}} \right)^2 + \frac{(N^{\rm tot}_{\rm dat} - N^{\rm tot}_{\rm exp}(\vec{p},\vec{\alpha}))^2}{N^{\rm tot}_{\rm dat}} + \sum_k \left(\frac{\alpha_k - \mu_k}{\sigma_k} \right)^2 \right\} , \tag{7}$$

for KamLAND. Since KamLAND used only one detector, we use directly the number of events per bin, $N_{{\rm dat},i}$ and $N_{{\rm exp},i}$. Following the collaboration, we include a penalty term on the total number of events $N^{\rm tot}_{\rm dat} = \sum_{i=1}^{N_{\rm KL}} N_{{\rm dat},i}$ and equivalently for the predicted number of events. The statistical analyses discussed here have been performed using the GLoBES software [14, 15].

We first discuss the result using only short baseline data. In fig. 2 we compare the result from the analysis without decoherence (colored regions) with the results obtained after marginalizing over the wave-packet width σ (black lines) in the $\sin^2\theta_{13} - \Delta m^2_{31}$ plane for the analysis of data from RENO (left), Daya Bay (central) and from the combination of the two (right). As can be seen, the determination of the parameters becomes much worse in presence of decoherence effects. This behavior could have been expected from fig. 1, where we saw that small values of the wave-packet width result in a suppression of the oscillation amplitude (which can be compensated with a larger

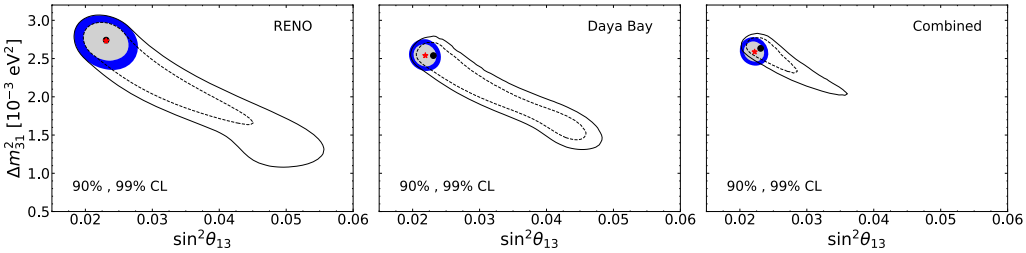

Fig. 2. – 90 and 99% CL (2 d.o.f.) allowed regions in the $\sin^2\theta_{13}$–Δm^2_{31} plane for RENO (left), Daya Bay (center) and the combination of both experiments (right). Filled regions correspond to the analyses assuming a perfectly coherent source, while black lines are obtained after marginalizing over σ. The best-fit points from the standard analyses are indicated with a red star, while the best-fit values from the analyses including σ are denoted by black dots.

mixing angle) and in a shift of the oscillation minimum to larger values in energy (which can be compensated with a smaller mass splitting). These correlations are also shown in fig. 3. From the combined analysis of RENO and Daya Bay data we can set a lower bound on the neutrino wave-packet width at $\sigma > 1 \times 10^{-4}$ nm. As was shown in fig. 1 (central panel), a value corresponding to the lower bound would completely wash out the oscillation minimum at KamLAND. We can therefore expect a better sensitivity from the analysis of KamLAND data. Since the minimum and maximum are not shifted, we can also expect that no strong correlations appear among the solar mass splitting and the wave-packet width. As can be seen in fig. 1 the bound that can be obtained by KamLAND (blue line) is indeed better than the one obtained from short baseline experiments. After combining all data we obtain the red line, which corresponds to $\sigma > 2 \times 10^{-4}$ nm. The sensitivity is clearly driven by the KamLAND data. Note that although we obtain a finite best fit value for the wave packet width, arbitrarily large values of σ remain allowed at 90% confidence level. Finally, after combining all reactor data we obtain the contours presented in fig. 5. All parameters not plotted have been

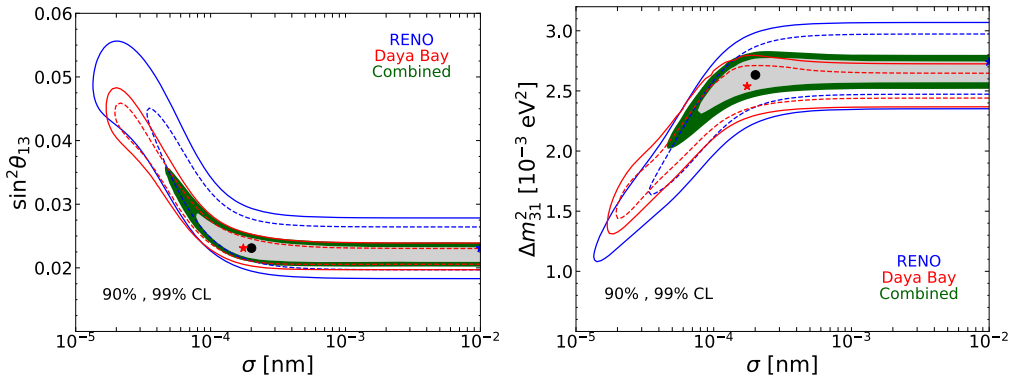

Fig. 3. – 90 and 99% CL (2 d.o.f.) allowed regions in the σ–$\sin^2\theta_{13}$ (left) and σ–Δm^2_{31} (right) planes for RENO (blue lines), Daya Bay (red lines) and the combination of the two (filled regions). Stars denote the best-fit values from the analysis of a single experiment on its own (the best-fit value for RENO lies at $\sigma \sim 10^{-2}$ nm), while the black dot is the best-fit point obtained from the combined analysis.

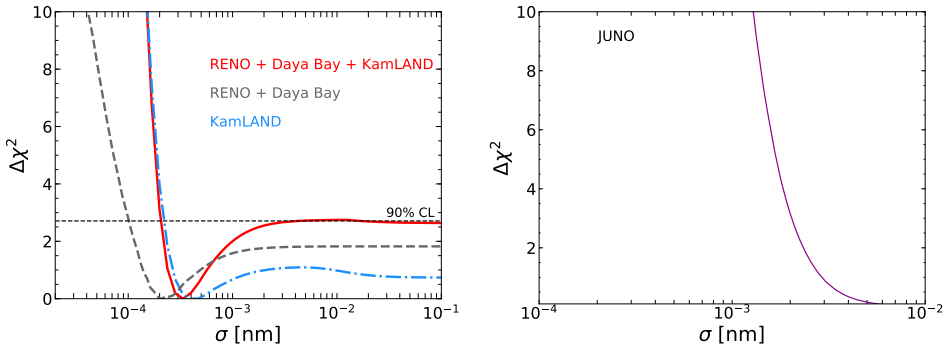

Fig. 4. – Left: The reduced χ^2 as a function of σ relative to its minimum value, obtained from the combined analysis of RENO, Daya Bay and KamLAND (red, solid) and from the combined analysis of only short-baseline experiments (grey, dashed). Right: The sensitivity at JUNO after 8 years of data taking. All standard oscillation parameters have been marginalized over.

marginalized over. The black lines are obtained in the standard analysis without decoherence effects, while the filled regions are obtained after marginalizing additionally over the wave-packet width. As can be seen in the right panel, the inclusion of KamLAND data helps to break the degeneracies among $\sin^2\theta_{13}$, Δm^2_{31} and σ, which we saw in fig. 3. The small values of σ which are correlated with large (small) values of $\sin^2\theta_{13}$ (Δm^2_{31}) are disfavored now and hence the degeneracy is broken. We find that the best fit value for $\sin^2\theta_{13}$ is shifted a bit, and that the region is a slightly larger, but the measurement can be regarded as robust. In the left panel we see that the presence of decoherence does not affect the measurement of Δm^2_{21}. However, it does impact the determination of $\sin^2\theta_{12}$. Values close to maximal mixing are now allowed within 1σ and also the best fit point is shifted closer towards maximal mixing. The reason is the same as before: finite values of the wave-packet width reduce the oscillation amplitude, which can be compensated with a larger mixing angle. Note, however, that the $\sin^2\theta_{12}$ measurement from solar data is much more precise and not effected by σ, since neutrinos coming from the sun are always treated as "perfectly incoherent". We can therefore conclude that the measurement of the standard oscillation parameters is fairly robust under the decoherence scenario.

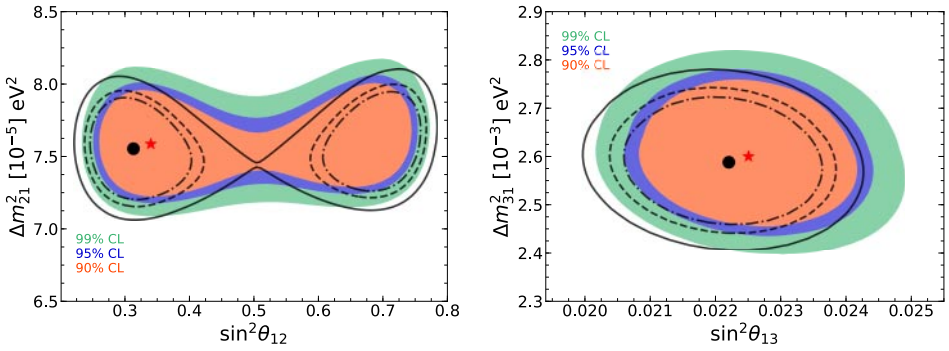

Fig. 5. – 90, 95 and 99% CL (2 d.o.f.) allowed regions in the $\sin^2\theta_{12}$-Δm^2_{21} (left) and $\sin^2\theta_{13}$-Δm^2_{31} (right) planes from our combined analysis of RENO + Daya Bay + KamLAND data including decoherence (filled regions, red stars) and assuming a perfectly coherent source (black empty contours, black dots).

4. – Sensitivity at future experiments

We also studied the sensitivity to the wave-packet width at JUNO([1]). For the experimental setup we followed the description presented in ref. [17], in particular we used the 10-reactor configuration. However, two of the reactors will probably not become operational [18], and therefore the sensitivity that we reported in ref. [1] could be achieved after 8 years (instead of 6 years) of data taking. Our statistical analysis is performed with

$$\chi^2_{\rm JUNO}(\vec{p}) = \min_{\vec{\alpha}} \left\{ \sum_{i=1}^{N_{\rm JUNO}} \left(\frac{N_{{\rm dat},i} - N_{{\rm exp},i}(\vec{p},\vec{\alpha})}{\sigma_i^{\rm JUNO}} \right)^2 + \sum_k \left(\frac{\alpha_k - \mu_k}{\sigma_k} \right)^2 \right\} , \tag{8}$$

where the fake data $N_{{\rm dat},i}$ were generated with the best fit point reported in ref. [19]. The result of this sensitivity study is shown in the right panel of fig. 4. The best fit point obtained in the analysis of current data lies well within the sensitivity reach of JUNO. Overall we find that JUNO can set $\sigma > 2 \times 10^{-3}$ nm at 90% CL, one order of magnitude stronger than the current bound.

5. – Conclusions

We performed a combined analysis of short and long baseline reactor antineutrino data in presence of decoherence effects. We found that current data can exclude wave-packet sizes $\sigma < 2 \times 10^{-4}$ nm at 90% confidence level, assuming that neutrinos from all nuclear-reactor cores can be characterized by the same σ. We also studied the impact of allowing for arbitrary values of σ when measuring $\sin^2\theta_{12}$, $\sin^2\theta_{13}$, Δm^2_{21}, and $|\Delta m^2_{31}|$. We found that, given the existing reactor data, these measurements are fairly robust. We found that KamLAND data are more sensitive to decoherence effects than in the cases of Daya Bay and RENO. This is not a trivial statement, since Daya Bay and RENO have accumulated more statistics and since KamLAND measures neutrinos from a plurality of nuclear cores and averaging-out effects, which tend to mimic those of decoherence, are very significant. It turns out, however, that the access to very long baselines, the relatively large value of $\sin^2 2\theta_{12}$, and the fact that KamLAND "sees" both oscillation maxima and minima leads to stronger sensitivity. In the next few years, we expect an order-of-magnitude better sensitivity from the JUNO experiment.

We have chosen not to add to the very interesting but subtle discussion of expectations for σ given antineutrinos produced in nuclear-reactor cores. Naive estimates are safely larger than the experimental bounds that we have obtained. Nonetheless, we find it is important to test the hypothesis that nuclear reactors are, for modern practical applications, a coherent source of antineutrinos, to probe how large decoherence effects could be, and to understand how these might impact our ability to measure fundamental physics parameters with reactor neutrino oscillation experiments.

* * *

Work supported by the research grant "The Dark Universe: A Synergic Multimessenger Approach" number 2017X7X85K under the program "PRIN 2017" funded by the Ministero dell'Istruzione, Università e della Ricerca (MIUR).

([1]) See also ref. [16].

REFERENCES

[1] de Gouvea A., de Romeri V. and Ternes C. A., *JHEP*, **08** (2020) 018.
[2] De Gouvêa A., De Romeri V. and Ternes C. A., arXiv:2104.05806 (2021).
[3] Giunti C., Kim C. and Lee U., *Phys. Rev. D*, **44** (1991) 3635.
[4] Giunti C., Kim C. and Lee U., *Phys. Lett. B*, **274** (1992) 87.
[5] Beuthe M., *Phys. Rev. D*, **66** (2002) 013003.
[6] Kayser B. and Kopp J., arXiv:1005.4081 (2010).
[7] de Salas P. F., Forero D. V., Gariazzo S., Martínez-Miravé P., Mena O., Ternes C. A., Tórtola M. and Valle J. W. F., *JHEP*, **02** (2021) 071.
[8] Denton P. B., Minakata H. and Parke S. J., *JHEP*, **06** (2016) 051.
[9] Barenboim G., Denton P. B., Parke S. J. and Ternes C. A., *Phys. Lett. B*, **791** (2019) 351.
[10] Adey D. *et al.*, *Phys. Rev. Lett.*, **121** (2018) 241805.
[11] Yoo J., *Reno* (2020), `https://doi.org/10.5281/zenodo.4123573`.
[12] *Kamland* (2010), `https://www.awa.tohoku.ac.jp/KamLAND/4th_result_data_release/4th_result_data_release.html`.
[13] Gando A. *et al.*, *Phys. Rev. D*, **83** (2011) 052002.
[14] Huber P., Lindner M. and Winter W., *Comput. Phys. Commun.*, **167** (2005) 195.
[15] Huber P., Kopp J., Lindner M., Rolinec M. and Winter W., *Comput. Phys. Commun.*, **177** (2007) 432.
[16] Cheng Z., Wang W., Wong C. F. and Zhang J., *Nucl. Phys. B*, **964** (2021) 115304.
[17] Aartsen M. *et al.*, *Phys. Rev. D*, **101** (2020) 032006.
[18] Abusleme A. *et al.*, arXiv:2005.08745 (2020).
[19] de Salas P. F., Forero D. V., Ternes C. A., Tortola M. and Valle J. W. F., *Phys. Lett. B*, **782** (2018) 633.